

JGR Space Physics

RESEARCH ARTICLE

10.1029/2021JA029569

Key Points:

- Chorus waves tend to be incoherent when the spatial extent is greater than 433 km or the time lag lasts 10 s at $< \sim 6.5$
- The spatial scale size of chorus wave is relatively larger near noon or with lower geomagnetic activity
- The temporal scale size of chorus wave is always statistically near zero, not influenced by L-shell, magnetic local time, or AL^* index

Supporting Information:

Supporting Information may be found in the online version of this article.

Correspondence to:

S. Zhang and A. M. Tian,
shuaizhang921125@qq.com;
tamin@sdu.edu.cn

Citation:

Zhang, S., Rae, I. J., Watt, C. E., J., Degeling, A. W., Tian, A., Shi, Q., et al. (2021). Determining the global scale size of chorus waves in the magnetosphere. *Journal of Geophysical Research: Space Physics*, 126, e2021JA029569. <https://doi.org/10.1029/2021JA029569>

Received 16 MAY 2021

Accepted 25 OCT 2021

Determining the Global Scale Size of Chorus Waves in the Magnetosphere

Shuai Zhang^{1,2} , I. Jonathan Rae^{1,3} , Clare E. J. Watt³ , Alexander W. Degeling¹ , Anmin Tian¹ , Quanqi Shi¹ , Xiao-Chen Shen⁴ , Shutao Yao¹ , Ruilong Guo¹ , Mengmeng Wang¹ , Xiaoqiong Zhu¹, and Huizi Wang¹

¹Shandong Provincial Key Laboratory of Optical Astronomy and Solar-Terrestrial Environment, Institute of Space Sciences, Shandong University, Weihai, China, ²Mullard Space Science Laboratory, University College London, London, UK, ³Department of Maths, Physics and Electrical Engineering, Northumbria University, Newcastle Upon Tyne, UK,

⁴Center for Space Physics, Boston University, Boston, MA, USA

Abstract Chorus waves outside the plasmapause influence the Earth's radiation belt dynamics by interacting with energetic electrons via cyclotron and Landau resonance. Recent numerical diffusion experiments indicate that the diffusion process is sensitive to the spatial and temporal scale of variability in the wave-particle interaction, which is reported to be more efficient than that based on the traditional average model. Using Van Allen Probes A and B data from November 2012 to July 2019, the spatial and temporal scale size of chorus waves are calculated by the correlation between the wave amplitudes detected by two satellites with varying spatial separation or time lag. We found that, the chorus wave is incoherent when the spatial extent is greater than 433 km or the time lag lasts ~ 10 s, which are significantly smaller than that of plasmaspheric hiss. In addition, the spatial correlations of chorus tend to be higher near noon or with lower geomagnetic activity. The temporal correlations of chorus are always statistically near zero, which are not influenced by the location and geomagnetic activity. Our results can help refine the model of the interactions between energetic particles and chorus waves in the radiation belt.

1. Introduction

Whistler mode waves play a significant role in Earth's radiation belt dynamics via wave-particle interactions. These interactions can lead to the acceleration of the trapped particle population, pitch angle and energy diffusions, and electron precipitations into the upper atmosphere (e.g., Li et al., 2019; Ni et al., 2013; Summers et al., 2007). Electrons will interact with several diverse whistler-mode waves in their drift orbits, such as chorus and plasmaspheric hiss (e.g., Agapitov et al., 2018; Meredith et al., 2006, 2012; Summers et al., 2007). Outside the plasmasphere, electrons encounter chorus waves, which are usually observed as a series of discrete elements in $0.1\text{--}0.8 f_{ce}$ (e.g., Koons & Roeder, 1990; Meredith et al., 2001; Santolík & Gurnett, 2003). These chorus waves are thought to be generated by the temperature anisotropy of injected energetic electrons (e.g., Omura et al., 2008, 2009). After generation, they can accelerate electrons to several MeV, cause electron precipitation through pitch angle scattering, and could be a significant embryonic source of plasmaspheric hiss (e.g., Bortnik et al., 2008, 2009; Meredith et al., 2013).

Traditional pitch angle diffusion models use parameterized diffusion coefficients that are mostly constructed from averaged plasma and wave properties (e.g., Fok et al., 2011; Horne et al., 2013; Tu et al., 2013). While, recent numerical experiments (Watt et al., 2019, 2021) indicate that the spatial and temporal variability of diffusion coefficients have universal importance for the diffusion process. Therefore, it is necessary to identify the temporal and spatial variation scale of wave characteristics to determine whether averaged diffusion coefficients can adequately capture the diffusion process, and to provide crucial information for use when constructing such averages.

For the plasmaspheric hiss waves, Zhang et al. (2021) has statistically studied the spatial and temporal scale size of plasmaspheric hiss by analyzing the correlation between the wave amplitudes detected by the two Van Allen Probes. They found the plasmaspheric hiss waves are statistically incoherent when spatial separation larger than $\sim 1,500$ km or temporal separation larger than ~ 10 min at $L < 4.5$, while it is always incoherent at $L > 4.5$. Zhang et al. (2021) therefore concluded that the plasmaspheric hiss could be

more variable than previously thought, and the statistical averages for the models of drift-averaged diffusion should be constructed with care. For the magnetospheric chorus waves, Santolík, Gurnett et al. (2003) and Santolík et al. (2004) analyzed the correlation of data from the four Cluster spacecraft at close separations during a geomagnetic storm, and found that the correlation scale of chorus elements varying between 60 and 200 km. Agapitov et al. (2017) found the spatial scale is about 600 km using 9 hr measurements onboard the Van Allen Probes. Aryan et al. (2016) statistically found the average scale size of chorus wave packets is to be about 1,300–2,300 km, by analyzing the difference in chorus wave amplitude (ΔB) observed by Van Allen Probe A and B. Using THEMIS satellites, Agapitov et al. (2018) statistically obtained the radial spatial scale of chorus waves is near 250–800 km, where the correlation of amplitudes drops to 0.5. Shen et al. (2019) statistically found the transverse correlation scale of chorus elements is about 315 km. In spite of these advances, the global spatial scale size of chorus waves in a physical coordinate system and its dependence on locations are still unclear. Specifically, the temporal scale size of chorus waves has not been studied statistically before, which has been revealed recently to be a significant factor for the radiation belt diffusion (Watt et al., 2021).

In this paper, similar to the analysis of hiss waves by Zhang et al. (2021), we study the temporal and spatial variability of chorus waves using two Van Allen Probes, which provide an ideal platform for this analysis through the constantly changing distance from ~ 0.01 to $5 R_E$, with probe A lapping probe B every several weeks. To be special, we statistically study the correlation of chorus wave amplitudes detected by two satellites against the satellite time lag and separation to identify the spatial and temporal variation scale of wave characteristics. Note that, this study focuses on the region of broader chorus activity, rather than the length scale of individual chorus elements. Section 2 details the data and analysis methods. The statistical results of chorus waves are shown in Section 3, followed by the discussions in Section 4 and conclusions in Section 5.

2. Data Description and Analysis Methods

2.1. Instruments

The measurements used in this study are obtained from the twin Van Allen Probes A and B, which are in nearly identical orbits with an apogee of $5.8 R_E$ (Mauk et al., 2012). The wave magnetic field data with $\sim 6s$ resolution used in this study are obtained from Electric and Magnetic Field Instrument Suite and Integrated Science (EMFISIS) onboard Van Allen Probes (Kletzing et al., 2013). In the Waveform Receiver data of EMFISIS, the singular value decomposition method is used to determine the wave normal angle, polarization, planarity, and ellipticity (Santolík, Parrot et al., 2003). The upper hybrid frequency detected by the High-Frequency Receiver spectra of EMFISIS is used to calculate the electron density (Kurth et al., 2015).

2.2. Selection Criteria

We select chorus waves using previously published criteria (e.g., Bingham et al., 2019; Hartley et al., 2019; Li et al., 2014), as follows:

- (1) Both Van Allen Probes A and B are outside the plasmapause, as determined by the electron density measurements are lower than the minimum value of 30 cm^{-3} and $10 \times (6.6/L)^4$.
- (2) The wave is in the typical chorus wave frequency range of $0.1\text{--}0.8 f_{ce}$, where f_{ce} is the equatorial electron gyrofrequency.
- (3) The planarity larger than 0.6, so that less wave power outside the polarization plane.
- (4) The ellipticity larger than 0.7 and polarization larger than 0.5, to ensure that the observed waves are right-handed circularly polarized whistle-mode waves.

2.3. Case Study

Figure 1 shows the summary of observations from Van Allen Probe A on January 20, 2013 as an example of how we derive our measurements. Continuously chorus wave activities were observed from 02:00–05:30 UT to 09:00–14:30 UT. Panel (a) shows the electron density measurements (blue line), and the horizontal dashed black line indicates the minimum value of 30 cm^{-3} and $10 \times (6.6/L)^4$. We can see that, the blue line

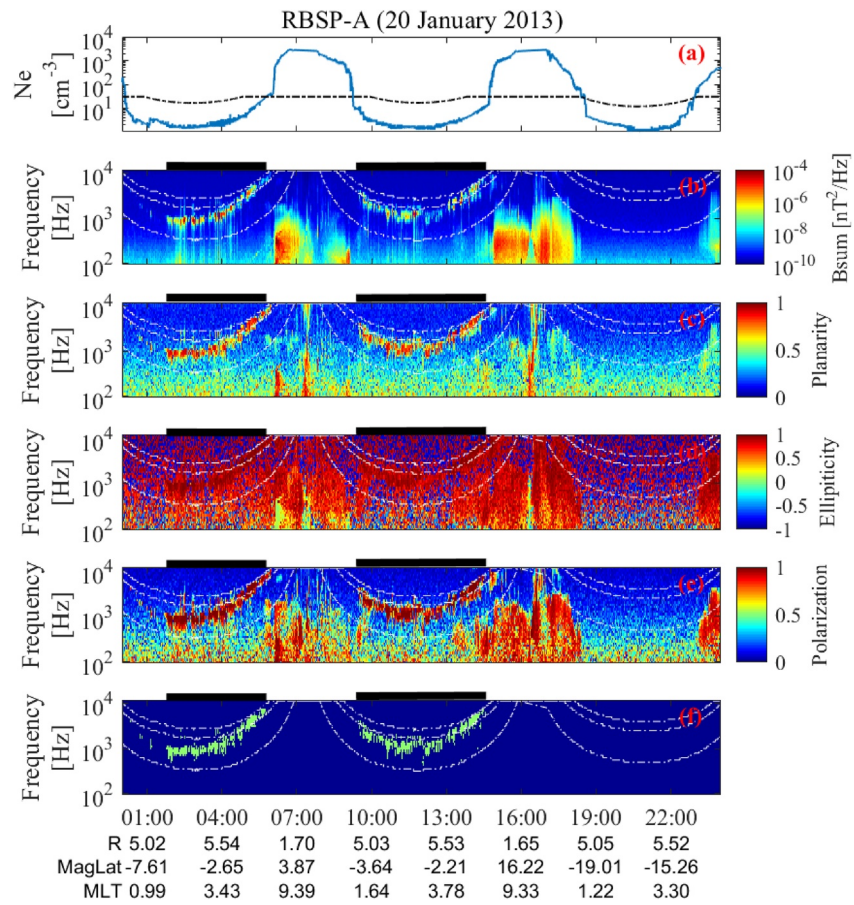


Figure 1. The density and magnetic field observations on January 20, 2013 from Van Allen Probes A. (a) Electron density. (b–e) Magnetic power spectral density, planarity, ellipticity, and polarization. (f) Bins that meet all criteria 1–4. The three white lines in panels (b–f) represent 0.1, 0.5, and $0.8 f_{ce}$. The black bars at the top of each panel indicate the duration of chorus waves.

is below the black line around 00:00–6:00 UT, 09:00–15:00 UT, and 19:00–23:00 UT, where the satellite is outside of the plasmasphere. Panel (b) shows the power spectral density of the magnetic field. It can be seen that some wave activities stay in $0.1\text{--}0.8 f_{ce}$ (upper and lower white lines) around 02:00–05:30 UT and 09:00–14:30 UT, while some wave activities near 07:00 UT and 16:00 UT do not meet criteria 1 and 2 (and are presumably therefore hiss waves). Panels (c–e) show the distributions of planarity, ellipticity, and polarization. We can determine where criteria 3 and 4 are met from these panels. Finally, the bins that meet all criteria 1–4 are shown in green in Figure 1f, and the black bars at the top of each panel indicate the duration of chorus waves.

Figure 2 shows the correlation analysis for the chorus waves during 02:00–05:30 UT and 09:00–14:30 UT on January 20, 2013. Panels (a and b) show the magnetic spectral density detected by Van Allen Probes A and B. It can be seen that the chorus spectra from Van Allen Probes A&B seem to have a relatively good correlation visually. Panel (c) gives the wave amplitudes calculated from magnetic spectral densities in panels (a, red) and (b, blue), which are integrated within $0.1\text{--}0.8 f_{ce}$ and smoothed for 1 min. The 1-min smoothing process is to reduce the effects of the sharp and frequent changes (burst characteristic) of chorus wave amplitudes. We can see that, the red and blue lines also appear in similar shapes and amplitudes. Panels (d and e) show the constantly varying spatial distance (Δd) and time lag between two satellites. The spatial separation is calculated from $\Delta d = \sqrt{\Delta x^2 + \Delta y^2 + \Delta z^2}$, where Δx , Δy , and Δz are the separations of two satellites in the three-axis directions of the GSE coordinate system. The time lag between two satellites arriving at the same place one after another can be estimated from the locations in panels (j and l). Note that, although the orbits of the two satellites are approximately the same, probe B does not arrive at exactly the same location as

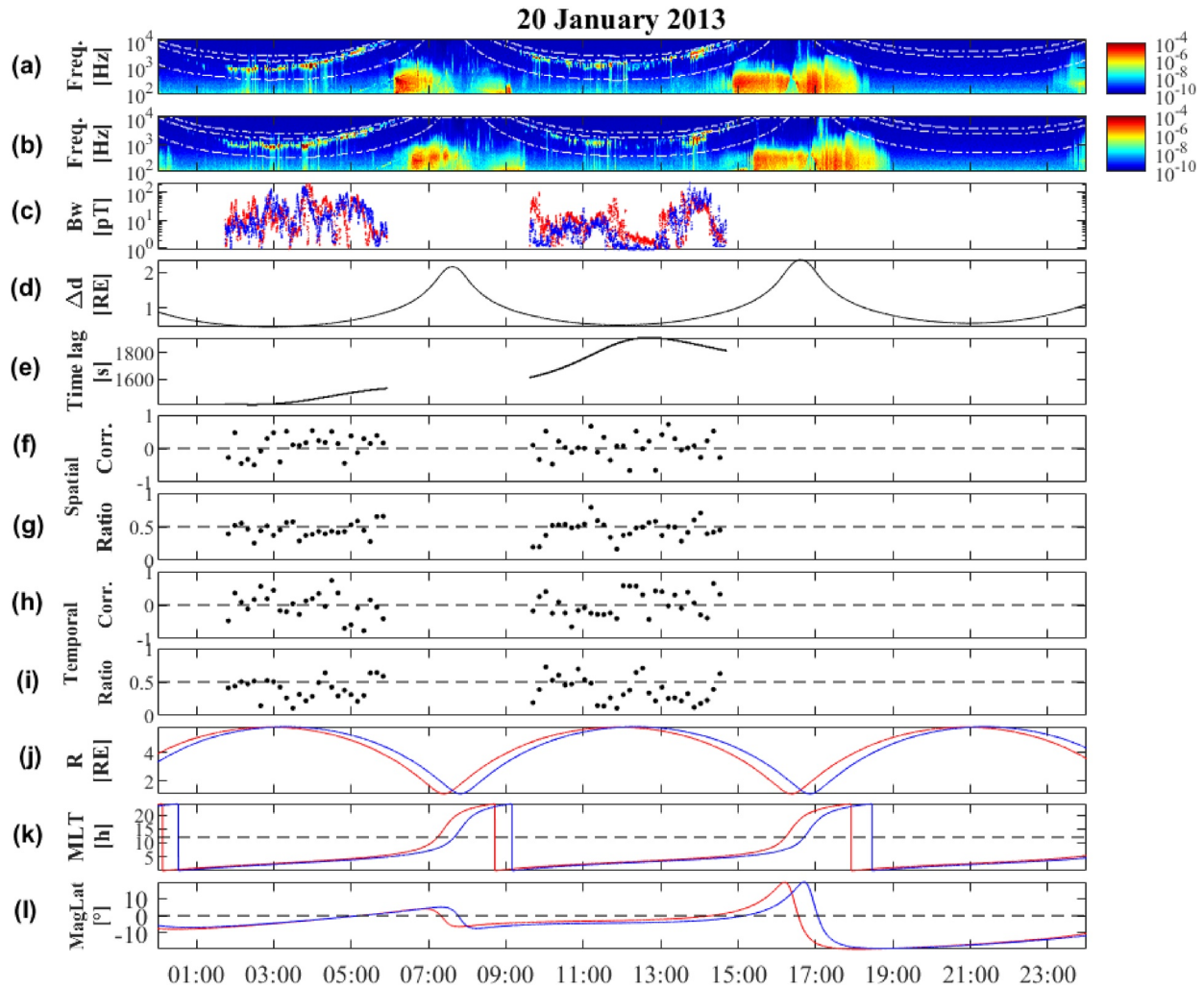


Figure 2. The correlation analysis of the chorus waves detected from Van Allen Probes on January 20, 2013. (a) Magnetic power spectral density detected by Van Allen Probes A and (b) B. The three white lines denote 0.1 , 0.5 , and $0.8 f_{ce}$. (c) The integrated chorus wave amplitudes from panels (a, red) and (b, blue). (d–e) The spatial distance and time lag between two satellites. (f and g) Spatial correlations and ratios of chorus wave amplitudes. (h and i) Temporal correlations and ratios of chorus wave amplitudes. (j–l) The locations of two satellites. The red and blue line indicates the measurements of Van Allen Probes A and B, respectively. R = radial distance from earth; MLT = magnetic local time; MagLat = magnetic latitude.

probe A, especially after 2016. Therefore, to calculate the time lag between two satellites, we first need to find the nearest position P on the orbit of probe B from probe A. Then, the time taken by probe B to reach position P is the time lag between the two satellites, and the separation between satellite A and position P is the orbital separation of the two satellites at this moment. Panels (f and g) display the calculated spatial correlations and ratios (smaller values/larger values) between two lines in panel (c) in 10-min steps. Panels (h and i) display the temporal correlations and ratios, which are also calculated from two lines in panel (c), but shifting the blue line by the time lag in panel (e). The reason for using a 10-min window is that we need to use as long a time window as possible for the study, while ensuring that the span of satellite position is small (less than $0.5 R_E$) during this time window. We can see that there is a significant variability both in the spatial and temporal correlations and amplitude ratios in panels (f–i). Using Van Allen Probes data from November 2012 to July 2019, a total of 3,875 events (each corresponding to a 10-min time window) were discovered, where the spatial distance between two satellites was less than $1 R_E$.

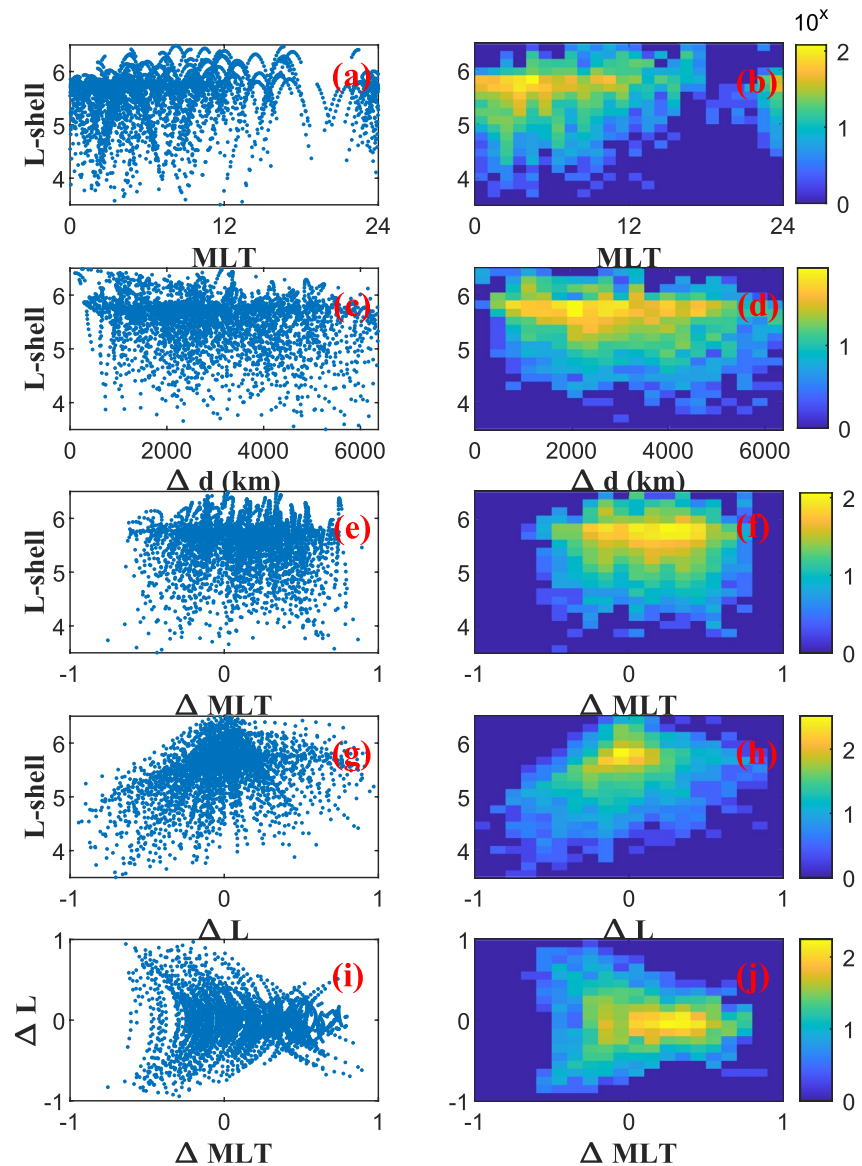


Figure 3. The scattered distribution of chorus wave events of magnetic local time MLT (a), total separation Δd (c), azimuthal separation ΔMLT (e), and radial separation ΔL (g) as the L-shell changes. (i) The scattered distribution of chorus wave events in ΔMLT - ΔL . The number distributions of chorus waves in left panels are shown in right panels.

3. Statistical Results

We use a similar method to Zhang et al. (2021), which studied the spatial and temporal scale size of plasmaspheric hiss wave, to analyze chorus waves. First, we analyze the distribution of locations and satellite separations for all 3,875 events. Then, the spatial correlations calculated in Figure 2f for all events are statistically studied, which are binned by Δd , L-shell, magnetic local time (MLT), and the geomagnetic activity index. Subsequently, the temporal correlations calculated in Figure 2h for 1,067 events with orbital separation less than 750 km are analyzed in the same way.

3.1. Distribution

Figure 3 displays the scatterplot (left-hand column) and number distribution (right-hand column) as a function of location and relative separations between RBSP A&B for all of 3,875 chorus waves. Panel (a) describes the distribution of chorus waves in the MLT-L plane, and panel (b) gives their number distribution

in a two-dimensional histogram. We can see that only a few chorus wave events are observed near dusk (MLT ~ 18). Except for duskside, the data shows a good coverage (>10 points) between $4.5 < L < 6$, and peaks at $5.5 < L < 6$. Panels (c and d) illustrate the wave distribution of the spatial distance (Δd) as the L-shell changes. We can also see that the distribution is well covered at $L > 4.5$, and peaks near $L \sim 5.5$ – 6 . It can be seen that our events almost evenly cover all spacecraft separations when $\Delta d < 1R_E$. Panels (e and f) illustrate the wave distributions of interspacecraft distance between two satellites in azimuthal direction (ΔMLT) as the L-shell changes. Panels (g and h) illustrate the wave distributions of interspacecraft distance between two satellites in the radial direction (ΔL) as the L-shell changes. It can be seen that, the chorus waves are concentrate in $|\Delta MLT| < 0.5$ hr and $|\Delta L| < 0.5$. Finally, panels (i and j) describe the distributions of chorus wave events in ΔMLT - ΔL . It can be seen that the chorus waves are concentrated near $\Delta L = 0$ and $\Delta MLT = 0.25$ hr.

3.2. Spatial Correlations of Chorus Waves

Figures 4a–4d illustrate the distribution function of spatial correlations in Figure 2f versus the spatial distance Δd of two satellites for 3,875 chorus wave events. Panel (a) describes the scattered distribution of the spatial correlations of chorus waves. Panel (b) gives the corresponding number distribution of the scattered points by the two-dimensional histogram. Panel (c) displays the probability distribution for each column in panel (b), and the largest number in a given column is normalized to 1. Panel (d) shows the results of bilinear interpolation on panel (c). We can see that, the spatial correlation coefficient of chorus waves between two satellites decreases significantly as the separation Δd increases. To quantify this variation, the fitting of peaks in correlations is represented by the red line in panel (d). Since, the correlations change from ~ 1 at $\Delta d \sim 0$ to 0 as Δd gets very large both theoretically and statistically, we choose the weights fitting formula as $f(\Delta d) = e^{k\Delta d}$, where $k = -0.0016$ and $R^2 = 0.54$. The weights are the total number of events in each column in Figure 4b. In the end, we calculated that the spatial correlations decrease to 0.5 at $\Delta d = 433$ km. It should note that the distribution of spatial ratios in Figure 2g also shows the trend of significantly decreasing with the increase of Δd , as shown in supplement Figures S1a–S1d.

Figures 4e–4p illustrate the distribution of spatial correlations versus of L-shell (e–h), MLT (i–l), and geomagnetic activity index AL^* (m–p), with a similar format in panels (a–d). AL^* indicates the minimum AL index in the previous 3 hr. It can be seen that, the spatial correlations tend to be higher at $L \sim [6,6.5]$, near noon, or with lower geomagnetic activity.

3.3. Temporal Correlations of Chorus Waves

As described in Section 2.3, although the orbits of the two satellites are approximately the same, probe B does not arrive at exactly the same location as probe A. This will lead to the results of temporal scale size may be affected by the spatial variations if we used all chorus wave events. Therefore, to reduce the effect of spatial variation on the results of temporal scale size, we assume that the length scale could be negligible to study the temporal scale size if the orbital separation of two satellites is less than 750 km (the spatial correlation is 0.3).

The distributions of the temporal correlations for 1,067 events with orbital separation less than 750 km are investigated in Figure 5, with a similar format in Figure 4. Panels (a–d) display the temporal correlations versus time lag of two satellites in Figure 2h. We can see that, the temporal correlations of chorus waves have a similar variation trend with that in Figures 4a–4d, and it decreased significantly with the increase of time lag. The fitting of peaks in temporal correlations is indicated as the red line in panel (d) with the fitting formula ($f(\Delta t) = e^{\lambda\Delta t}$), where $\lambda = -0.067$ and $R^2 = 0.56$. It can be calculated that the temporal correlations decrease to 0.5 when $\Delta t = 10$ s. It should note that the distribution of temporal ratios in Figure 2g also shows the trend of significantly decreasing with the increase of Δt , as shown in supplement Figures S1e–S1h. Panels (e–p) show the impact of L-shell, MLT, and AL^* on the temporal correlations of chorus wave. It can be seen that the temporal correlations are always statistically near zero, and not influenced by L-shell, MLT, and AL^* index.

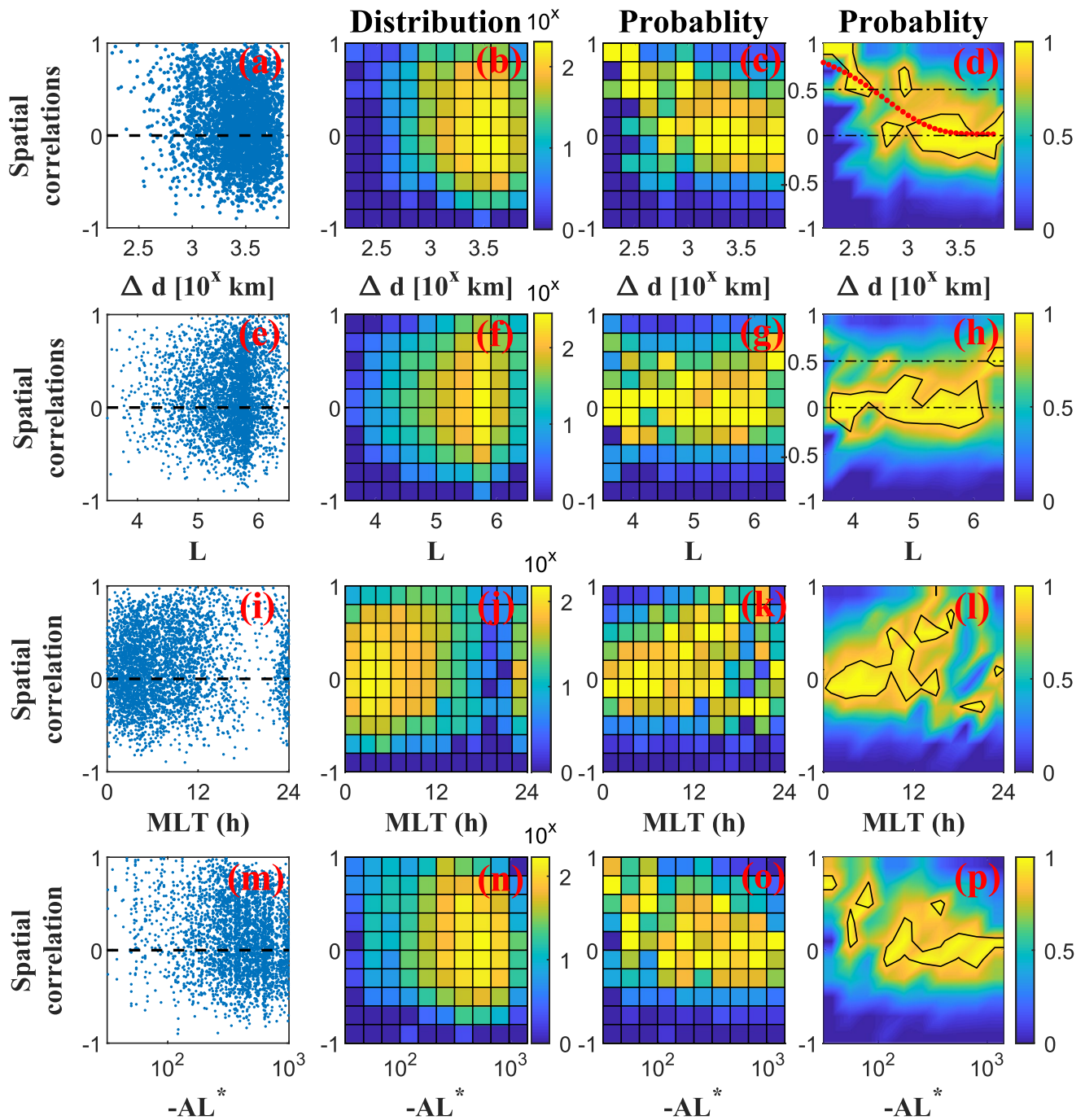


Figure 4. Distribution functions of the spatial correlations of chorus waves. The upper panels illustrate the scattered distribution (a), the number distribution (b), the probability distribution (c), and the interpolated probability distribution (d) of the spatial correlations of chorus waves versus the spatial distance Δd of two satellites. The black solid lines are the 0.9 contours of the interpolated distribution, and the red line represents the fitting ($f(\Delta d) = e^{\lambda \Delta d}$) to these contours. The lower panels illustrate the distributions of the spatial correlations of chorus waves versus L-shell (e–h), magnetic local time (i–l), and AL^* (m–p) with a similar format in panels (a–d).

4. Discussion

Using observations of Van Allen Probes A and B from November 2012 to July 2019, we statistically studied the global scale size of chorus waves. 3,875 chorus waves are found using established criteria (e.g., outside the plasmasphere, $0.1\text{--}0.8 f_{ce}$, higher planarity, polarization, and ellipticity). Most of the events are

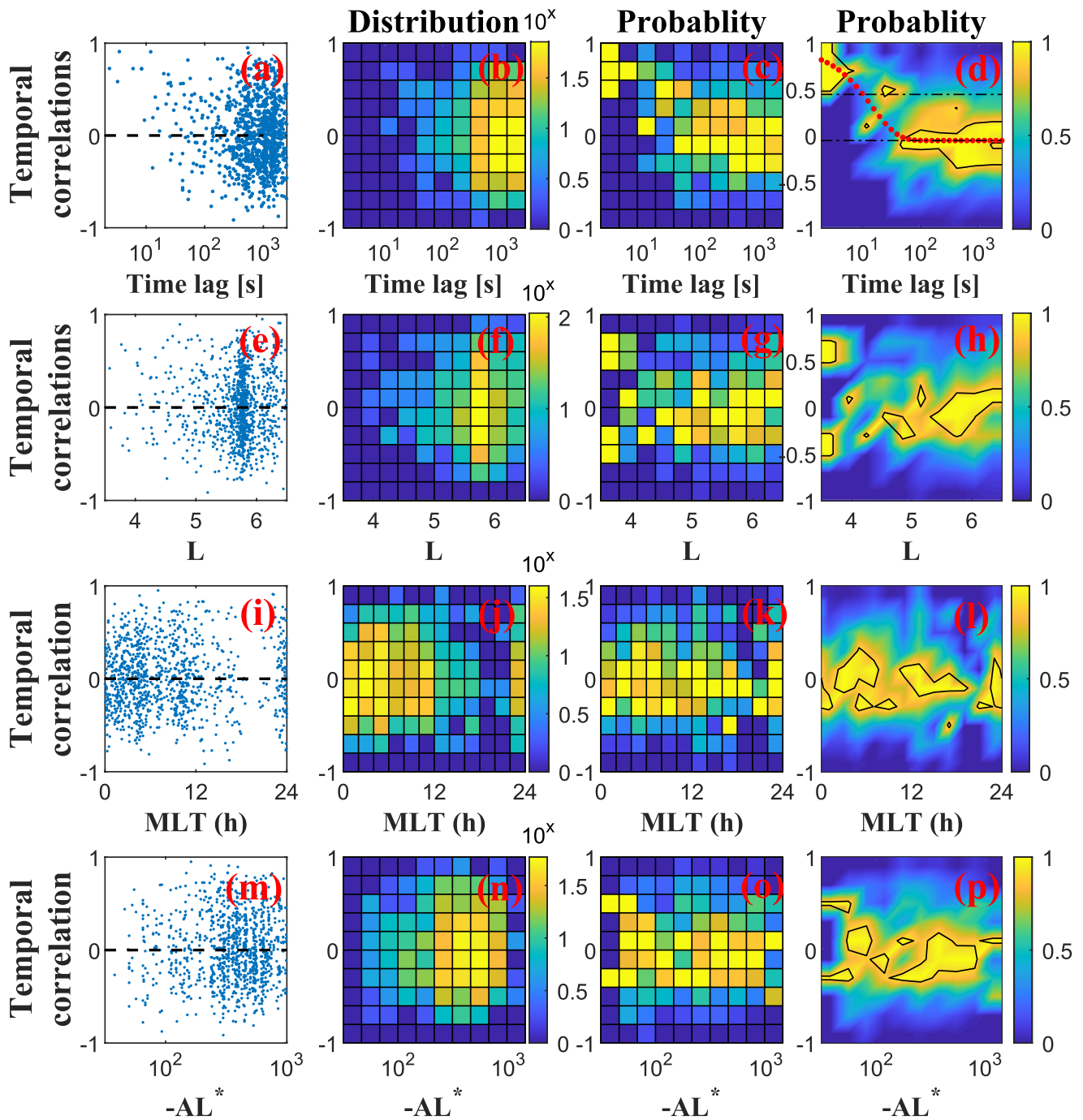


Figure 5. The distributions of the temporal correlations versus Time lag (a–d), L -shell (e–h), magnetic local time (i–l), and AL^* (m–p), which have the same format as Figure 4.

distributed at $L > 4.5$, and only a few chorus wave events are detected on the duskside. This is because chorus waves are typically generated from the injected energetic electrons outside the plasmapause, and these electrons injected near midnight from substorm and drifting around down to the dayside will cause the duskside is unfavorable for chorus generation (e.g., Meredith et al., 2012).

4.1. Spatial Scale Size of Chorus Waves

Figures 4a–4d show the correlations drop to 0.5 when separation (Δd) up to ~ 433 km, which means the statistically spatial scale size of chorus wave is ~ 433 km. Interestingly, Shen et al. (2019) showed that the correlation of chorus elements drops to 0.5 when the transverse separation (Δ_{\perp}) up to 450 km, which was similar to our results for the chorus waves. Agapitov et al. (2018) obtained that the correlation of chorus amplitudes drops to 0.5 near $250 < \Delta r < 800$ km using five THEMIS spacecraft observations, which is also consistent with our result. Moreover, it can be seen that the spatial scale size of chorus wave is significantly smaller than that of plasmaspheric hiss ($\sim 1,500$ km) shown by Zhang et al. (2021). This is consistent with the traditional concept that the hiss waves are more uniform than the chorus waves.

Figures 4e–4h show that the spatial correlations are higher at large L . However, Figure 3c shows that the closest conjunctions ($\Delta d < 287$ km) between two satellites also just happen to occur at higher L ($L > 6.2$), which could drive correlation values up at higher L in Figures 4e–4h. Therefore, to further judge this conclusion, we plot the distributions of the spatial correlation coefficients as a function of the spacecraft separation Δd and L-shell, as shown in Figure 6. We can see that the correlation at large L is not significantly different from the other regions. This suggests that the L-shell has no significant effect on the spatial scale size. Figure 4i–4l shows the spatial scale size is relatively higher at dayside than nightside, which is also similar to the conclusion of Shen et al. (2019) and Agapitov et al. (2018). Figures 6c and 6d also show that the correlations near noon are significantly larger than the other regions. This may be due to the injected electrons with different drift speeds drifting from the nightside to the dayside and spreading wider, resulting in the spatial regions of chorus generation being relatively wider and more uniform on the dayside (Agapitov et al., 2018). Figures 4m–4p show the spatial scale size is higher at low AL*. Figures 6e and 6f also show that the correlations at lower geomagnetic activity are significantly larger than the other regions. This could be understood that the magnetosphere should be more stable when the geomagnetic index is lower; the magnetosphere is less variable without substorm activity to disturb the current magnetospheric state.

4.2. Temporal Scale Size of Chorus Waves

The temporal scale size of chorus waves has not been studied statistically and quantitatively before. Recent numerical experiments demonstrate that, the temporal variability is very important for diffusion models due to the wave-particle interactions (Thompson et al., 2020; Watt et al., 2019, 2021). Figures 5a–5d show the temporal correlations are proportional to time lag ($e^{-0.0067 * \Delta t}$) and drops to 0.5 when $\Delta t = 10$ s, which means the statistically temporal scale size of chorus wave only lasts ~ 10 s, and could be negligible compared to the electron diffusion timescales. Moreover, Figures 5e–5p show that the temporal scale size is not influenced by the L-shell, MLT, or geomagnetic index, which are different from the spatial scale size. This may be due to the fact that, the chorus wave is statistically temporal-incoherent at all L-shell, MLT, or AL* bins. Moreover, we can see that the temporal scale size of chorus wave is significantly smaller than that of plasmaspheric hiss (~ 10 min) shown by Zhang et al. (2021), which is also consistent with the traditional concept that the chorus waves are patches in the magnetosphere while hiss waves are relatively uniform.

Numerical experiments demonstrate that the solution of Fokker-Planck equation for the diffusion model is sensitively dependent on the temporal variability of the diffusion coefficient (Thompson et al., 2020; Watt et al., 2021), which will be affected by the spatial and temporal variations of the wave and plasma parameter. Watt et al. (2021) performed multiple numerical experiments of bounce-averaged diffusion, and indicated that rapid variations (with timescales of ~ 2 min) of whistler-mode wave diffusion coefficients resulted in solutions of the Fokker-Planck equations that were similar to results obtained from an averaged diffusion coefficient. For much longer timescales (~ 6 hr), results from averaged experiments did not match well with the results from experiments with temporally varying coefficients. There is therefore good reason to investigate the temporal and spatial variability of waves to determine whether averaged diffusion coefficients are an accurate description of the diffusive process; if diffusion coefficients can be successfully averaged, then they are constants, and can be calculated once and implemented in a simple deterministic parameterization. The alternative is to have to construct temporally varying diffusion coefficients that realistically encompass all the variation possible in the observationally constrained diffusion coefficients (see Watt et al., 2021), and run the Fokker-Planck simulations as ensembles. Given how many different types of wave particle interactions there are, these ensembles could become unwieldy and intractable very quickly.

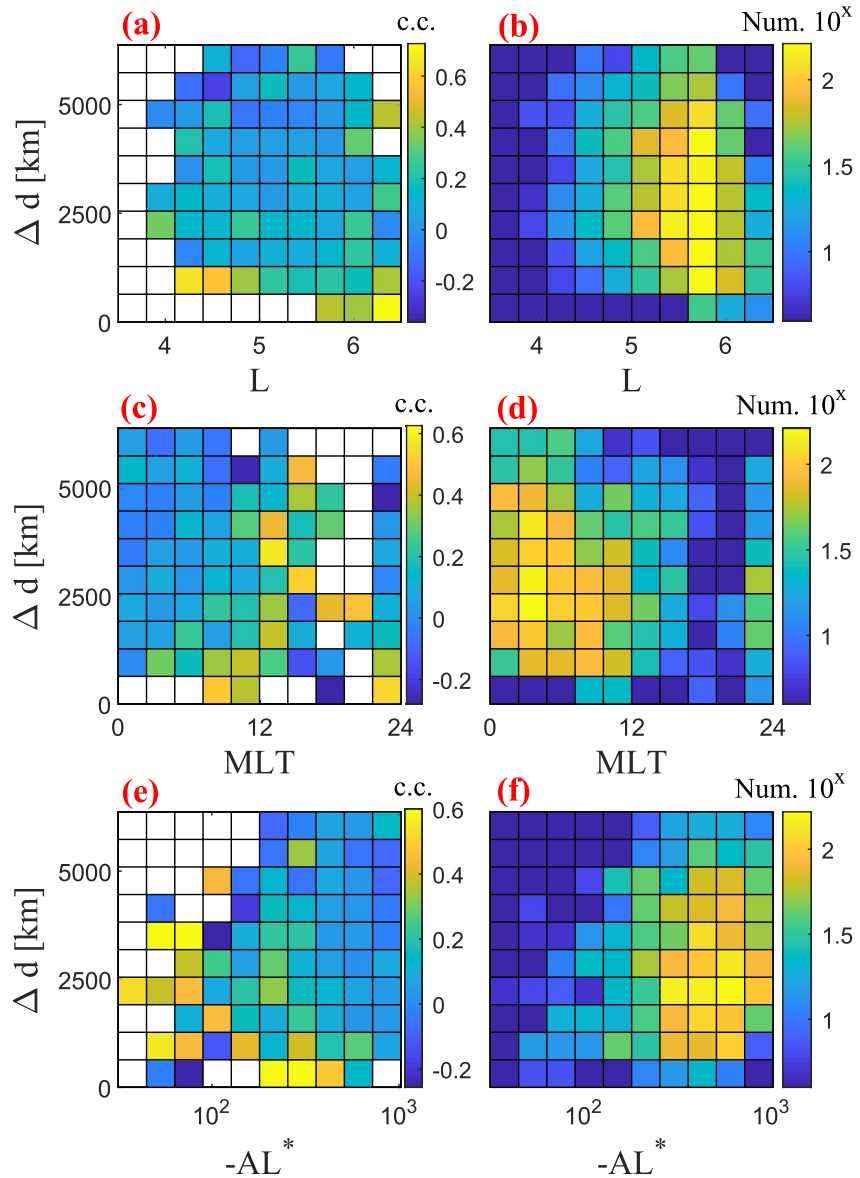


Figure 6. (a) The distributions of the spatial correlation coefficients as a function of the spacecraft separation Δd and L-shell. The color indicates the median value of the spatial correlation coefficients in each bin. (b) The number of events in each bin. (c–f) The distributions of the spatial correlation coefficients as a function of the spacecraft separation Δd and magnetic local time and AL^* , with the same format as that in panels (a and b).

Importantly, when constructing averaged diffusion coefficients, the average should be obtained by combining multiple observation-specific diffusion coefficients (see Ross et al., 2020; Watt et al., 2019) rather than constructing diffusion coefficients from separately averaged wave parameters and plasma parameters. The results presented in this paper help us to consider how to construct drift-averages of diffusion coefficients from observations, once individual observation-specific bounce-averaged diffusion coefficients have been constructed.

When considering the temporal scales of varying diffusion that a radiation belt electron experiences, we must consider the temporal scale of variation of waves and plasma parameters in a particular location as well as the spatial scales of regions of wave activity that the electron travels through on its drift path. Figure 7 indicates the drift speed V_d (panel a) and drift period T_d (panel b) of electrons at $L = 5$ versus electron energy, which can be calculated by (Chisham, 1996; Li et al., 1993; Zhang et al., 2019):

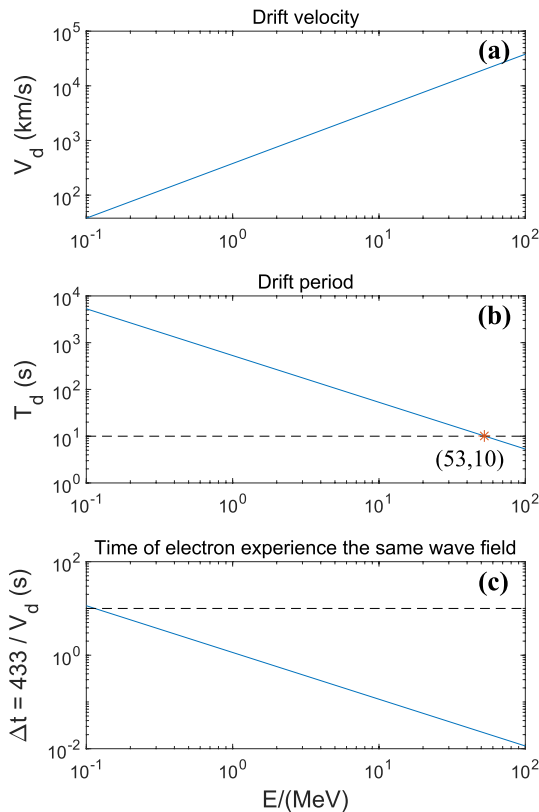


Figure 7. (a) The drift speed of electron; (b) the drift period of electron; and (c) the time of electron experience the same wave. The dashed lines indicate the period of 10 s, which is the temporal scale size of chorus wave.

$$V_d = -\frac{3L^2WR_E^2(0.7 + 0.3\sin\alpha)}{qk_0}; T_d = \frac{2\pi \cdot LR_E}{V_D}$$

where W is the electron energy, α is the equatorial pitch angle, k_0 is the magnetic moment of Earth's dipole.

For all energies less than 53 MeV, the chorus waves are likely to have changed significantly by the time the electron drifts around the Earth and encounters the same region of space again. Panel (c) shows the amount of time that electrons with each energy would spend in a spatial region of waves as the electron drifts around the Earth. The extent of the spatial region is 433 km, as shown above, although this could signify the maximum likely extent of the wave activity region, since we are considering here that the spatial scale is largest in the azimuthal direction (drift direction). For all energies studied (100 keV–100 MeV), electrons will spend a very short time traversing the wave activity region in comparison to the length of time that the activity region persists. These results indicate that the spatial variation of the wave activity, and the plasma parameters such as number density, are just as important for calculating the drift-averaged diffusion coefficient as the temporal variations themselves.

The timescales of electron interaction with different small spatial regions of chorus are very short (see Figure 7c) ranging from around 10 s at $E = 100$ keV to around 0.5 s at $E = 2$ MeV, and around 0.1 s at $E = 10$ MeV. This suggests that when constructing a drift-average, an average of observation-specific bounce-averaged coefficients is likely to work well, since the effective timescales for electrons drifting through chorus wave regions are very short. Further numerical experiments, similar to those in Watt et al. (2021), but using an appropriate distribution of chorus diffusion coefficients constructed as in Watt et al. (2019) should confirm whether the timescales indicated in Figure 7c are short enough to allow for straightforward averaging.

5. Summary and Conclusions

Using observations of Van Allen Probes A and B from November 2012 to July 2019, we studied the spatial and temporal scale size of 3,875 chorus waves by calculating the correlation between the wave amplitudes detected by two satellites with varying spatial separation or time lag. The main results are summarized as follows:

- (1) Chorus waves tend to be incoherent when the spatial extent is greater than 433 km or the time lag lasts 10 s at $L < \sim 6.5$, which are significantly smaller than that of plasmaspheric hiss ($\sim 1,500$ km and ~ 10 min);
- (2) Chorus wave is more spatially -coherent near noon or with lower geomagnetic activity;
- (3) Chorus wave is statistically temporally -incoherent at $L < \sim 6.5$, and does not depend on location or geomagnetic activity;

These results show how the chorus wave amplitudes vary in space and time considering the influence of locations and geomagnetic activity, which will be used to refine the model of interactions between energetic particles and waves in the radiation belt. Timescales indicate that drift-averaging of observation-specific diffusion coefficients for chorus waves is likely to be an effective and accurate way to describe the wave-particle interaction. In the future, the temporal and spatial variability of all other inputs for diffusion coefficient calculations that can also be analysis to build a more realistic model.

Data Availability Statement

We acknowledge the use of the Van Allen Probes data at <https://spdf.sci.gsfc.nasa.gov/>.

Acknowledgments

This work was funded by the National Natural Science Foundation of China (Grants 41961130382, 41974189, and 41731068), the Royal Society Newton Advanced Fellowship (NAF/R1/191047), and the Shandong University (Weihai) Future Plan for Young Scholars (2017WHWLJH08). I. J. Rae was funded by the Natural Environment Research Council (NE/V002724/1, NE/V002554/1, NE/P017185/1, and NE/P017150/1) and the Science and Technology Facilities Council (ST/V006320/1). C. E. J. Watt was funded by the NERC (grant NE/P017274) and the STFC (grant ST/R000921/1). X.-C. Shen was funded by the NASA (grants 80NSSC20K0698, 80NSSC20K0557, NNX17AD15G, and 80NSSC20K1270).

References

- Agapitov, O., Blum, L. W., Mozer, F. S., Bonnell, J. W., & Wygant, J. (2017). Chorus whistler wave source scales as determined from multipoint Van Allen Probe measurements. *Geophysical Research Letters*, *44*, 2634–2642. <https://doi.org/10.1002/2017GL072701>
- Agapitov, O., Mourenas, D., Artemyev, A., Mozer, F. S., Bonnell, J. W., Angelopoulos, V., et al. (2018). Spatial extent and temporal correlation of chorus and hiss: Statistical results from multipoint THEMIS observations. *Journal of Geophysical Research: Space Physics*, *123*, 8317–8330. <https://doi.org/10.1029/2018JA025725>
- Aryan, H., Sibeck, D., Balikhin, M., Agapitov, O., & Kletzing, C. (2016). Observation of chorus waves by the Van Allen Probes: Dependence on solar wind parameters and scale size. *Journal of Geophysical Research: Space Physics*, *121*, 7608–7621. <https://doi.org/10.1002/2016JA022775>
- Bingham, S. T., Moukikis, C. G., Kistler, L. M., Paulson, K. W., Farrugia, C. J., Huang, C. L., et al. (2019). The storm time development of source electrons and chorus wave activity during CME- and CIR-driven storms. *Journal of Geophysical Research: Space Physics*, *124*, 6438–6452. <https://doi.org/10.1029/2019JA026689>
- Bortnik, J., Li, W., Thorne, R. M., Angelopoulos, V., Cully, C., Bonnell, J., et al. (2009). An observation linking the origin of plasmaspheric hiss to discrete chorus emissions. *Science*, *324*, 775–778. <https://doi.org/10.1126/science.1171273>
- Bortnik, J., Thorne, R. M., & Meredith, N. P. (2008). The unexpected origin of plasmaspheric hiss from discrete chorus emissions. *Nature*, *452*, 62–66. <https://doi.org/10.1038/nature06741>
- Chisham, G. (1996). Giant pulsations: An explanation for their rarity and occurrence during geomagnetically quiet times. *Journal of Geophysical Research*, *101*(A11), 24757–24763. <https://doi.org/10.1029/96JA02540>
- Fok, M. C., Gloer, A., Zheng, Q., Horne, R., Meredith, N., Albert, J., & Nagai, T. (2011). Recent developments in the radiation belt environment model. *Journal of Atmospheric and Solar: Terrestrial Physics*, *73*, 1435–1443. <https://doi.org/10.1016/j.jastp.2010.09.033>
- Hartley, D. P., Kletzing, C. A., Chen, L., Horne, R. B., & Santolik, O. (2019). Van Allen Probes observations of chorus wave vector orientations: Implications for the chorus-to-hiss mechanism. *Geophysical Research Letters*, *46*, 2337–2346. <https://doi.org/10.1029/2019GL082111>
- Horne, R. B., Kersten, T., Glauert, S. A., Meredith, N. P., Boscher, D., Sicard-Piet, A., et al. (2013). A new diffusion matrix for whistler mode chorus waves. *Journal of Geophysical Research: Space Physics*, *118*, 6302–6318. <https://doi.org/10.1002/jgra.50594>
- Kletzing, C. A., Kurth, W. S., Acuna, M., MacDowall, R. J., Torbert, R. B., Averkamp, T., et al. (2013). The Electric and Magnetic Field Instrument Suite and Integrated Science (EMFISIS) on Van Allen Probes. *Space Science Reviews*, *179*, 127–181. <https://doi.org/10.1007/s11214-013-9993-6>
- Koons, H. C., & Roeder, J. L. (1990). A survey of equatorial magnetospheric wave activity between 5 and 8 R_E . *Planetary and Space Science*, *38*(10), 1335–1341. [https://doi.org/10.1016/0032-0633\(90\)90136-E](https://doi.org/10.1016/0032-0633(90)90136-E)
- Kurth, W. S., De Pascuale, S., Faden, J. B., Kletzing, C. A., Hospodarsky, G. B., Thaller, S., & Wygant, J. R. (2015). Electron densities inferred from plasma wave spectra obtained by the Waves instrument on Van Allen Probes. *Journal of Geophysical Research: Space Physics*, *120*, 904–914. <https://doi.org/10.1002/2014JA020857>
- Li, J., Ma, Q., Bortnik, J., Li, W., An, X., Reeves, G. D., et al. (2019). Parallel acceleration of suprathermal electrons caused by whistler-mode hiss waves. *Geophysical Research Letters*, *46*, 12675–12684. <https://doi.org/10.1029/2019GL085562>
- Li, W., Mourenas, D., Artemyev, A. V., Agapitov, O. V., Bortnik, J., Albert, J. M., et al. (2014). Evidence of stronger pitch angle scattering loss caused by oblique whistler-mode waves as compared with quasi-parallel waves. *Geophysical Research Letters*, *41*, 6063–6070. <https://doi.org/10.1002/2014GL061260>
- Li, X., Hudson, M., Chan, A., & Roth, I. (1993). Loss of ring current O^+ ions due to interaction with Pc 5 waves. *Journal of Geophysical Research*, *98*, 215–231. <https://doi.org/10.1029/92JA01540>
- Mauk, B. H., Fox, N. J., Kanekal, S. G., Kessel, R. L., Sibeck, D. G., & Ukhorskiy, A. (2012). Science objectives and rationale for the Radiation Belt Storm Probes mission. *Space Science Reviews*, *179*, 3–27. <https://doi.org/10.1007/s11214-012-9908-y>
- Meredith, N. P., Horne, R. B., & Anderson, R. R. (2001). Substorm dependence of chorus amplitudes: Implications for the acceleration of electrons to relativistic energies. *Journal of Geophysical Research*, *106*(A7), 13165–13178. <https://doi.org/10.1029/2000JA900156>
- Meredith, N. P., Horne, R. B., Bortnik, J., Thorne, R. M., Chen, L., Li, W., & Sicard-Piet, A. (2013). Global statistical evidence for chorus as the embryonic source of plasmaspheric hiss. *Geophysical Research Letters*, *40*, 2891–2896. <https://doi.org/10.1002/grl.50593>
- Meredith, N. P., Horne, R. B., Clilverd, M. A., Horsfall, D., Thorne, R. M., & Anderson, R. R. (2006). Origins of plasmaspheric hiss. *Journal of Geophysical Research*, *111*, A09217. <https://doi.org/10.1029/2006JA011707>
- Meredith, N. P., Horne, R. B., Sicard-Piet, A., Boscher, D., Yearby, K. H., Li, W., & Thorne, R. M. (2012). Global model of lower band and upper band chorus from multiple satellite observations. *Journal of Geophysical Research*, *117*, A12209. <https://doi.org/10.1029/2012JA017978>
- Ni, B., Bortnik, J., Thorne, R. M., Ma, Q., & Chen, L. (2013). Resonant scattering and resultant pitch angle evolution of relativistic electrons by plasmaspheric hiss. *Journal of Geophysical Research: Space Physics*, *118*, 7740–7751. <https://doi.org/10.1002/2013JA019260>
- Omura, Y., Hikishima, M., Katoh, Y., Summers, D., & Yagitani, S. (2009). Nonlinear mechanisms of lower-band and upper-band VLF chorus emissions in the magnetosphere. *Journal of Geophysical Research*, *114*, A07217. <https://doi.org/10.1029/2009JA014206>
- Omura, Y., Katoh, Y., & Summers, D. (2008). Theory and simulation of the generation of whistler-mode chorus. *Journal of Geophysical Research*, *113*, A04223. <https://doi.org/10.1029/2007JA012622>
- Ross, J. P. J., Glauert, S. A., Horne, R. B., Watt, C. E. J., Meredith, N. P., & Woodfield, E. E. (2020). A new approach to constructing models of electron diffusion by emic waves in the radiation belts. *Geophysical Research Letters*, *47*, e2020GL088976. <https://doi.org/10.1029/2020gl088976>
- Santolik, O., & Gurnett, D. A. (2003). Transverse dimensions of chorus in the source region. *Geophysical Research Letters*, *30*(2), 1031. <https://doi.org/10.1029/2002GL016178>
- Santolik, O., Gurnett, D. A., & Pickett, J. S. (2004). Multipoint investigation of the source region of storm-time chorus. *Annales Geophysicae*, *22*(7), 2555–2563. <https://doi.org/10.5194/angeo-22-2555-2004>
- Santolik, O., Gurnett, D. A., Pickett, J. S., Parrot, M., & Cornilleau-Wehrlin, N. (2003). Spatio-temporal structure of storm-time chorus. *Journal of Geophysical Research*, *108*(A7), 1278. <https://doi.org/10.1029/2002JA009791>
- Santolik, O., Parrot, M., & Lefeuvre, F. (2003). Singular value decomposition methods for wave propagation analysis. *Radio Science*, *38*(1), 1010. <https://doi.org/10.1029/2000RS002523>

- Shen, X.-C., Li, W., Ma, Q., Agapitov, O., & Nishimura, Y. (2019). Statistical analysis of transverse size of lower band chorus waves using simultaneous multisatellite observations. *Geophysical Research Letters*, *46*, 5725–5734. <https://doi.org/10.1029/2019GL083118>
- Summers, D., Ni, B., & Meredith, N. P. (2007). Timescales for radiation belt electron acceleration and loss due to resonant wave-particle interactions: 1. Theory. *Journal of Geophysical Research*, *112*, A04206. <https://doi.org/10.1029/2006JA011801>
- Thompson, R. L., Watt, C. E. J., & Williams, P. D. (2020). Accounting for variability in ULF wave radial diffusion models. *Journal of Geophysical Research*, *125*. <https://doi.org/10.1029/2019JA027254>
- Tu, W., Cunningham, G. S., Chen, Y., Henderson, M. G., Camporeale, E., & Reeves, G. D. (2013). Modeling radiation belt electron dynamics during GEM challenge intervals with the DREAM3D diffusion model. *Journal of Geophysical Research: Space Physics*, *118*, 6197–6211. <https://doi.org/10.1002/jgra.50560>
- Watt, C. E. J., Allison, H. J., Meredith, N. P., Thompson, R. L., Bentley, S. N., Rae, I. J., et al. (2019). Variability of quasilinear diffusion coefficients for plasmaspheric hiss. *Journal of Geophysical Research: Space Physics*, *124*, 8488–8506. <https://doi.org/10.1029/2018JA026401>
- Watt, C. E. J., Allison, H. J., Thompson, R. L., Bentley, S. N., Meredith, N. P., Glauert, S. A., et al. (2021). The implications of temporal variability in wave-particle interactions in Earth's radiation belts. *Geophysical Research Letters*, *48*. <https://doi.org/10.1029/2020gl089962>
- Zhang, S., Rae, I. J., Watt, C. E. J., Degeling, A. W., Tian, A. M., Shi, Q. Q., et al. (2021). Determining the temporal and spatial coherence of plasmaspheric hiss waves in the magnetosphere. *Journal of Geophysical Research: Space Physics*, *126*. <https://doi.org/10.1029/2020JA028635>
- Zhang, S., Tian, A. M., Degeling, A. W., Shi, Q. Q., Wang, M. M., Hao, Y. X., et al. (2019). Pc4-5 Poloidal ULF wave observed in the dawnside plasmaspheric plume. *Journal of Geophysical Research: Space Physics*, *124*, 9986–9998. <https://doi.org/10.1029/2019JA027319>